


Article

Investigation of Elastic Properties of the Single-Crystal Nickel-Base Superalloy CMSX-4 in the Temperature Interval between Room Temperature and 1300 °C

Alexander Epishin ^{1,*}, Bernard Fedelich ^{2,*}, Monika Finn ², Georgia Künecke ², Birgit Rehmer ² , Gert Nolze ², Claudia Leistner ³, Nikolay Petrushin ⁴ and Igor Svetlov ⁴

¹ Faculty III Process Sciences, Institute of Material Sciences and Technology, Chair of Metallic Materials, Technische Universität Berlin, Sekr. BH18, Ernst-Reuter-Platz 1, 10587 Berlin, Germany

² Department of Materials Engineering, Federal Institute for Materials Research and Testing (BAM), Unter den Eichen 87, 12205 Berlin, Germany; monika.finn@bam.de (M.F.); georgia.kuenecke@bam.de (G.K.); birgit.rehmer@bam.de (B.R.); gert.nolze@bam.de (G.N.)

³ Institute Applied Materials, Helmholtz-Zentrum Berlin, for Materials and Energy, Hahn-Meitner-Platz 1, 14109 Berlin, Germany; claudia.leistner@helmholtz-berlin.de

⁴ All-Russian Institute of Aviation Materials (VIAM), Radio Str. 17, 105005 Moscow, Russia; nv_petrushin@mail.ru (N.P.); i.svetlov2010@yandex.ru (I.S.)

* Correspondence: a.epishin@tu-berlin.de (A.E.); bernard.fedelich@bam.de (B.F.); Tel.: +49-(0)30-314-78981 (A.E.); +49-(0)30-8104-3104 (B.F.)



Citation: Epishin, A.; Fedelich, B.; Finn, M.; Künecke, G.; Rehmer, B.; Nolze, G.; Leistner, C.; Petrushin, N.; Svetlov, I. Investigation of Elastic Properties of the Single-Crystal Nickel-Base Superalloy CMSX-4 in the Temperature Interval between Room Temperature and 1300 °C. *Crystals* **2021**, *11*, 152. <https://doi.org/10.3390/cryst11020152>

Academic Editors: Ronald W. Armstrong and Dmitry Lisovenko
Received: 26 December 2020
Accepted: 26 January 2021
Published: 2 February 2021

Publisher's Note: MDPI stays neutral with regard to jurisdictional claims in published maps and institutional affiliations.



Copyright: © 2021 by the authors. Licensee MDPI, Basel, Switzerland. This article is an open access article distributed under the terms and conditions of the Creative Commons Attribution (CC BY) license (<https://creativecommons.org/licenses/by/4.0/>).

Abstract: The elastic properties of the single-crystal nickel-base superalloy CMSX-4 used as a blade material in gas turbines were investigated by the sonic resonance method in the temperature interval between room temperature and 1300 °C. Elastic constants at such high temperatures are needed to model the mechanical behavior of blade material during manufacturing (hot isostatic pressing) as well as during technical accidents which may happen in service (overheating). High reliability of the results was achieved using specimens of different crystallographic orientations, exciting various vibration modes as well as precise measurement of the material density and thermal expansion required for modeling the resonance frequencies by finite element method. Combining the results measured in this work and literature data the elastic constants of the γ - and γ' -phases were predicted. This prediction was supported by measurement of the temperature dependence of the γ' -fraction. All data obtained in this work are given in numerical or analytical forms and can be easily used for different scientific and engineering calculations.

Keywords: nickel-base superalloys; single-crystals; characterization; elastic constants

1. Introduction

Blades of the hot section of gas turbines operate under severe service conditions including high temperatures, different mechanical loads, and an aggressive environment. In order to achieve the required service properties, the blades are solidified as single-crystals of nickel-base superalloys [1,2]. The excellent mechanical properties of nickel-base superalloys at high temperatures are provided by their two phase microstructure: The γ -solid solution of nickel strengthened by the γ' -precipitates, a phase on the base of the intermetallic compound Ni_3Al . Single-crystal blades are critical structural components of a gas turbine which determine the efficiency and reliability of the whole assembly. Therefore, the lifetime of turbine blades has to be reliably predicted by rigorous engineering calculations, which includes modeling the mechanical behavior of a blade material. Two types of mechanical models can be applied for this purpose: The models treating a blade material as a homogeneous continuum [3–5] and the advanced physically-based models explicitly considering the two phase γ/γ' -microstructure of nickel-base superalloys [6–10]. In particular, models of the last type have been developed to predict microstructural evolutions at

high temperatures like rafting [6,7,9,10]. Both types of models require numerous material parameters, the first models at a macroscopic level, that is the parameters of a material as a whole, and the second models at a microscopic level, that is separately the parameters of the constituent γ - and γ' -phases. This set of mechanical parameters also includes the characteristics of elasticity, which in the case of cubic crystals of nickel-base superalloys is described by three elastic constants, usually by the elastic stiffnesses c_{11} , c_{12} , and c_{44} .

It is important to adequately characterize the elastic properties of nickel-base superalloys because they are highly anisotropic. For example, in [11] the elastic properties of the single-crystal superalloy GS6F were reported. It was found that at room temperature (RT), the Zener factor of anisotropy $A = 2 c_{44} / (c_{11} - c_{12})$ is equal to about 2.5, while Young's modulus E_x and shear modulus G_{xy} change by a factor of about 2.2 depending on x - and y -directions with minimum for $E_{\langle 001 \rangle}$ and $G_{\langle 011 \rangle \langle 01\bar{1} \rangle}$, and maximum for $E_{\langle 111 \rangle}$ and $G_{\langle 001 \rangle \langle hk0 \rangle}$, ($G_{\langle 001 \rangle \langle hk0 \rangle}$, is independent of $\langle hk0 \rangle$). The most anisotropic characteristic is Poisson's ratio ν_{xy} , which even inverts its sign changing from the maximum value $\nu_{\langle 011 \rangle \langle 100 \rangle} = +0.65$ to the minimum value $\nu_{\langle 011 \rangle \langle 01\bar{1} \rangle} = -0.06$ [12]. A detailed analysis of the extreme values of the Poisson ratio of cubic crystals can be found in [13].

Under normal service conditions, the maximum operating temperature of blade material does not exceed 1150 °C, therefore the elastic constants of nickel-base superalloys are usually measured at temperatures up to this limit [13–17]. However, in some specific cases, the elastic constants at higher temperatures are needed. One such case is modeling technical accidents when the blade material can experience a short γ' -solvus overheating [18]. Another case is modeling hot isostatic pressing (HIP) [19,20] which is performed in a temperature window between the γ' -solvus and solidus where the strengthening γ' -phase is totally dissolved and therefore the superalloy is very soft [21]. Such modeling activities need elastic constants at temperatures up to about 1300 °C. Therefore, the first objective of our work was measuring the macroscopic elastic constants of the single-crystal nickel-base superalloy CMSX-4 in a temperature interval between RT and 1300 °C.

As mentioned above, the advanced physically-based models for the mechanical behavior of single-crystal nickel-base superalloys require microscopic elastic constants separately for the γ - and γ' -phases. Knowledge of these microscopic parameters is also of academic interest, namely for understanding the phenomenon of rafting the initially cuboidal γ' -precipitates that occurs in superalloy under high temperature creep conditions. This phenomenon was first considered by Tien and Copley [22] and then investigated in many publications, e.g., analytically by Pineau [23] or by means of transmission electron microscopy (TEM) by Svetlov et al. [24]. Nabarro [25] reviewed available publications on rafting and proposed the “elastic concept for rafting”, which predicts the direction of γ' -rafting depending on the sign of the product $m \times \delta$, where δ is the misfit of γ - and γ' -lattice spacing and m is the misfit of the elastic moduli of the γ - and γ' -phases. Nabarro defined m as:

$$m = \frac{(M^p - M^m)}{0.5 (M^p + M^m)} \quad (1)$$

where $M = c_{11} - c_{12}$. From here and below we will use the superscripts “m” and “p” respectively for the γ -matrix and γ' -precipitates. According to this elastic concept for rafting during creep under uniaxial $\langle 001 \rangle$ tensile loading the γ' -phase forms rafts normal to load axis (N-rafting) if $m \times \delta < 0$ and rafts parallel to load axis (P-rafting) if $m \times \delta > 0$. N-rafting is usually observed in Ni-base alloys where $\delta < 0$ [26,27], while P-rafting is often observed in Co-base alloys where $\delta > 0$ [28,29]. Many experimental efforts were made to clarify the sign of m for nickel-base superalloys [16,30–34]. However, until now there is no full agreement about this point in the literature. Therefore, the second objective of this work is the prediction of the elastic properties of the γ - and γ' -phases of CMSX-4 as well as $\text{sign}(m)$.

The determination of the macroscopic and microscopic elastic constants requires certain material parameters, such as the density and temperature dependencies of thermal

expansion and volume fraction of γ' -phase. Therefore, the third objective of this work was the precise measurements of these characteristics for superalloy CMSX-4.

2. Materials and Methods

2.1. Investigated Specimens

The investigated material was the single-crystal nickel-base superalloy CMSX-4 [35] developed by Cannon-Muskegon, Muskegon, USA and is widely used as blade material for aircraft jet engines and land-based gas turbines. The single-crystals of different crystallographic orientations were solidified by Doncasters Precision Castings (DPC), Bochum, Germany, and were fully heat treated and used for different experiments performed in this work. For measurement of the elastic constants, 3 plate-shaped, rectangular specimens were cut by spark erosion. The plate-shaped beams were 3 mm thick, 8 mm wide, and 80 mm long, and had the following orientations: 1st beam-axial [001] with side faces (100) and (010); 2nd beam-axial [011] with wide and narrow side faces respectively (100) and (01 $\bar{1}$); and 3rd beam-axial [111] with wide and narrow side faces respectively ($\bar{2}11$) and (01 $\bar{1}$). The exact crystallographic orientations (Euler angles) of the specimens were measured by two methods: X-ray diffraction (XRD), the Laue method, and by a metallographic method, as described in ([2] chapter 4.4). The metallographic method is based on an analysis of the orientation of dendritic structure visualized on the specimen surface by macro etching. An advantage of this method is that the orientation can be examined across the entire surface of the specimen. As was shown in [21], the difference between the results of XRD and the metallographic method is within 1–3°, which is comparable with the misorientation of subgrains in “technical single-crystals” of nickel-base superalloys, see e.g., [36,37].

2.2. Measurement of Elastic Constants

The elastic constants of heat treated CMSX-4 have been determined by the sonic resonance (SR) method developed by Förster [38]. The principle of the SR method and its application to isotropic materials is described in detail in the ASTM E1875 standard [39]. The SR-measurements have been performed under vacuum in a testing device Elastotron 2000 HTM, Reetz, Berlin, Germany at temperatures between 24 °C and 1300 °C. The holding times varied from 5 min to 20 min depending on the temperature. A special measurement temperature was 1280 °C because it is the γ' -solvus temperature of CMSX-4. Therefore, at 1280 °C and 1300 °C the elastic constants of the γ -matrix of CMSX-4 were measured.

The frequency spectra of different flexural and torsional vibration modes were registered in the range between 1 kHz and 70 kHz. Harmonics of the orders between 4th and 7th were excited depending on the vibration mode, the specimen orientation, and temperature. Figure 1 shows an example of the lower parts (1–20 kHz) of the frequency spectra measured for the [001] beam of CMSX-4 at 24 and 1300 °C.

An interpretation of the resonance frequency peaks is possible by solving the eigenvalue problem for free dynamic vibrations with given elastic constants. For example, the computed resonance modes for the [001] specimen at 24 °C are shown in Figure 2. Note that at 24 °C, the 6th resonance peak is due to the first torsional mode, while at 1300 °C the first torsional mode corresponds to the 7th peak (see Figure 1).

In the case of isotropic materials, closed-form solutions for the eigenfrequencies can be applied to estimate the elastic constants from the resonance peaks (see e.g., [39]). Since shear and bending modes are generally coupled for anisotropic materials, sufficiently accurate analytical estimates of the eigenfrequencies are not available for arbitrary oriented crystals. Therefore, in this work the eigenfrequencies have been calculated by finite element analysis (FEA, see, e.g., [40]) and with the Abaqus FE code [41].

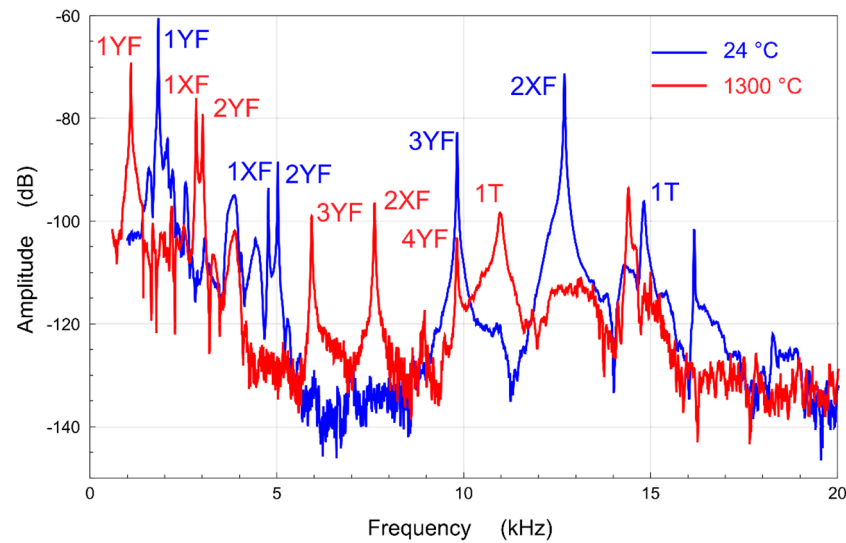


Figure 1. Lower parts (1–20 kHz) of frequency spectra measured from the [001] beam of CMSX-4 at 24 and 1300 °C. T-torsional peaks, and Y- and X-flexural peaks.

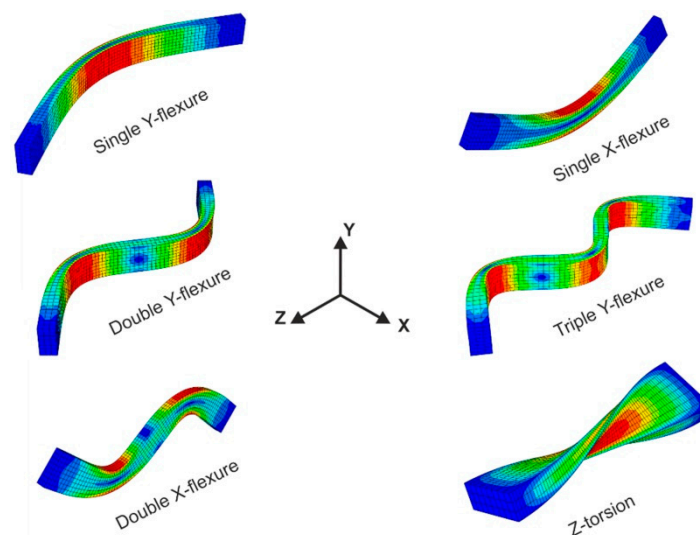


Figure 2. The first six resonance modes of the [001] beam at 24 °C.

The Lanczos solver of Abaqus has been applied to compute the eigenfrequencies of the freely oscillating beams. A mesh made of $3 \times 8 \times 80 = 1920$ quadratic elements (20 nodes, Abaqus type C3D20) was found to ensure a relative accuracy better than 5×10^{-4} for the computed eigenfrequencies. The mesh can be also seen in Figure 2. The unknown elastic constants $\{p_i\} = \{c_{11}, c_{12}, c_{44}\}$ were determined by minimizing the sum $R(p_i)$ of the squares of the deviations between measured and calculated peak frequencies (Least Square Method), that is,

$$R(p_i) = \sum_{s=1}^3 \frac{1}{2 N_s} \sum_{n=1}^{N_s} \left(\frac{f_{sn}^{FE}(p_i) - f_{sn}^{Exp}}{f_{sn}^{Exp}} \right)^2 \quad (2)$$

where N_s is the number of considered resonance modes for the specimen s , f_{sn}^{Exp} the n^{th} measured resonance frequency of the same specimen, and $f_{sn}^{FE}(p_i)$ is the corresponding computed eigenfrequency. It should be stressed that the three tested specimens are considered in the sum of the deviations in Equation (2). The use of specimens of different orientations as well as a large number of vibration modes is necessary to improve the reliability of the results. However, with increasing order and temperature the identification

of the resonance peaks becomes increasingly uncertain, which in practice limits the number of available experimental resonance frequencies. As a rule, all resonance peaks up to the first torsional mode have been taken into account in the objective function $R(p_i)$. In accordance, the first 6 or 7 modes and the first 4 modes have been considered in the case of the [001] specimen, respectively in the case of the [011] and [111] specimens. An exception was the [011] specimen at 1300 °C, for which the 4th resonance peak could not be identified with certainty.

To assess the reliability of these results, the influence of imprecisions concerning the specimen orientations was investigated by applying perturbations to the specimen orientations. More specifically, additional rotations of 2° around a random axis were applied to each specimen. It was found that such perturbations induced an average relative error equal to 0.5% for c_{44} , 2% for c_{11} , and 4% for c_{12} .

2.3. Measurement of Material Density and Thermal Expansion

The calculation of the resonance frequencies needs the material density $\rho(T)$ at investigated temperatures. Therefore, the density of CMSX-4 at RT and the linear thermal expansion (LTE) $\varepsilon_T(T)$ were carefully measured. The density $\rho(RT)$ was measured by the Archimedes method, i.e., weighting the specimen in air and water. The specimens for density measurement were machined in cylindrical shape with a diameter of 18 mm, length of 45 mm, and a mass of about 100 g. Such massive specimens with a small ratio surface/volume are preferable for density measurements. To avoid gas bubbles attaching to the specimen surface during measurements in liquid, the corners of the cylinders were rounded and the surface polished very carefully. During the measurements, the temperature of air and water varied within ± 0.1 °C. The precision balance used, a Sartorius R160D, has an accuracy of 0.01 mg. The measurements gave the following density value $\rho(23 \text{ °C}) = 8.72 \pm 0.01 \text{ g/cm}^3$.

The LTE of CMSX-4 was measured under vacuum in a dilatometer DL 1500, Ulvac Sinku-Riko, Japan in the temperature range between 20 and 1310 °C. The measured dependence $\varepsilon_T(T)$ shown in Figure 3 is well approximated by Equation (3):

$$\varepsilon_T(T) = a + b T + c \exp(d T), \quad (3)$$

where $a = -6.66 \times 10^{-4}$; $b = 1.24 \times 10^{-5}$, °C⁻¹; $c = 1.34 \times 10^{-4}$, and $d = 3.28 \times 10^{-3}$, °C⁻¹. The γ' -solvus temperature of CMSX-4 determined by a kink point in the curve $\varepsilon_T(T)$ was found to be $T_S = 1280 \pm 2$ °C, see insert in Figure 3. The temperature change of density was calculated as $\rho(T) = \rho(RT)/[1 + \varepsilon_T(T)]^3$. Raw data for $\varepsilon_T(T)$ are given in Appendix A.

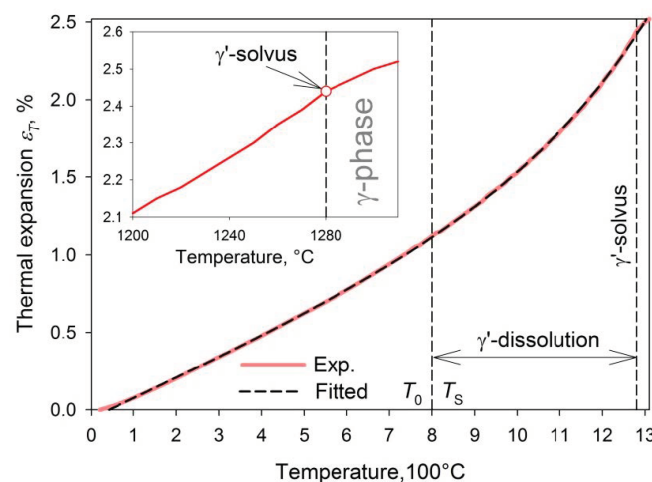


Figure 3. Thermal expansion of CMSX-4. The red solid line is the measured dilatometric curve and the black dashed line is the approximation with Equation (3). Kink of the dilatometric curve shown in the insert indicates the γ' -solvus temperature of CMSX-4 equal to 1280 °C.

2.4. Measurement of the Temperature Dependence of γ' -Volume Fraction

In this work the elastic constants of the γ' -phase were predicted using those of the γ -matrix and γ/γ' -compound. These calculations need reliable data for the temperature dependence of the γ' -volume fraction of CMSX-4 $f^P(T)$. Different methods are applied to measure the γ' -volume fraction in nickel-base superalloys, namely: Scanning electron microscopy (SEM) of the γ/γ' -microstructure [42,43], chemical extraction of the γ' -phase [44], XRD [44], electron probe X-ray microanalysis (EPMA) of the compositions of γ - and γ' -phases in TEM [45,46], measurement of the alloy electrical resistivity [47], and others. However, nearly all these methods do not provide reliable results with an acceptable accuracy. For example, in [45,46] $f^P(RT)$ was measured in CMSX-4 by the same method, EPMA in TEM, but the reported results significantly differ, 68 vol.% in [45] and 78 vol.% in [46]. In our opinion the most reliable method to measure f^P is SEM analysis of the specimens with the pre-rafterd coarse γ/γ' -microstructure, as applied in [48,49]. Therefore, this method was used in this work. In order to form such a pre-rafterd γ/γ' -microstructure, a [001] single-crystal of CMSX-4 was aged under creep conditions at a low temperature, 900 °C, under low stress, 170 MPa, for a very long time, 6400 h. This creep test resulted in a pre-rafterd coarse γ/γ' -microstructure without a noticeable creep strain, see the 1st SEM image (at 900 °C) inserted in Figure 4. During pre-raftering, the width of the γ -channels w increased from about 50 nm to about 180 nm, as measured in [50]. It should be mentioned that according to the literature data [46,47] and the results of our investigations, the γ' -fraction in CMSX-4 at temperatures below 850–900 °C is nearly equal to that at RT, $f^P(900\text{ °C}) = f^P(RT)$. The pre-rafterd specimen was cross cut into several pieces which were heated up to different temperatures between 950 °C and 1250 °C, and held for 1 h (at 950–1100 °C) or 0.5 h (at 1150–1250 °C) in order to reach the equilibrium γ' -fraction. Then the high temperature γ/γ' -microstructure was frozen by water quenching. The quenched specimens were longitudinally cut along (100) crystallographic plane (perpendicular to the γ' -rafts) and prepared for SEM where the final step of fine polishing was performed with colloidal silica. Chemical etching was avoided to exclude the etching artefacts. The specimens were observed in a scanning electron microscope FEG-SEM GEMINI 1530 VP, LEO, Germany in backscattered electron (BSE) mode. A total of 12 BSE images were taken from every specimen and processed using the image processing program ImageJ [51]. The results are presented graphically in Figure 4 as circles as well as numerically in Table 1. The vertical error bars show the standard error of the mean value, which varies between 1 and 2 vol.% depending on the temperature. The red solid line is an analytical approximation. It was assumed that $f^P(T) = f^P(RT) = 74\text{ vol.}\%$ at temperatures T below $T_0 = 850\text{ °C}$ while at temperatures T between T_0 and $T_S = 1280\text{ °C}$ is described by

$$f^P(T_0 \leq T \leq T_S) = f^P(RT) \times \left[1 - \left(\frac{T - T_0}{T_S - T_0} \right)^n \right]^N, \quad (4)$$

where $n = 2.635$ and $N = 0.651$.

It is seen from Figure 4 that in the temperature range 850–1050 °C the results of this work are in agreement with the results measured in [46] by EPMA in TEM (blues squares).

Table 1. The γ' -volume fraction f^P as a function of temperature, vol. %.

$T, \text{ °C}$	900	950	1000	1050	1100	1150	1200	1250	1280
f^P	74.0	72.3	70.5	68.9	60.1	54.0	43.4	22.8	0

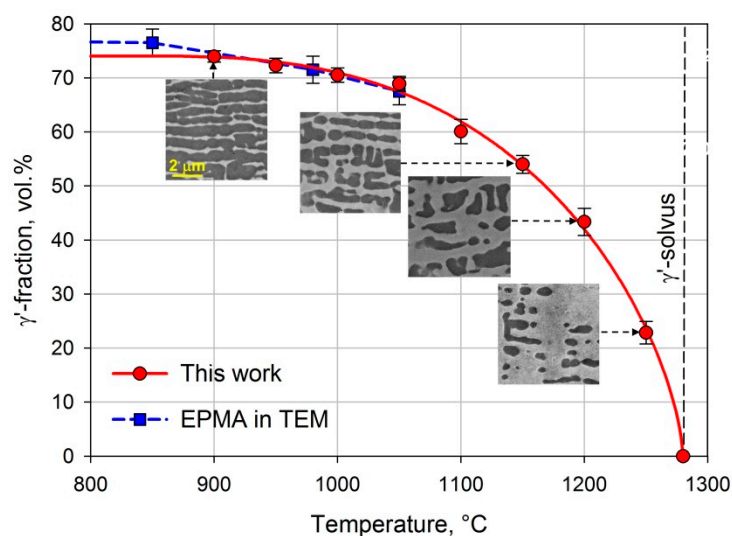


Figure 4. The γ' -volume fraction in CMSX-4 as a function of temperature. Blue squares and a blue dashed line—measured by electron probe X-ray microanalysis (EPMA) in transmission electron microscopy (TEM) in [46] (averaged for two deliveries of CMSX-4), and the red circles and red solid line (approximation with Equation (4))—in this work. Inserts are SEM images of the pre-rafted γ/γ' -microstructures quenched from investigated temperatures.

3. Results

3.1. Temperature Dependence of Elastic Constants of Superalloy CMSX-4

The components of the elastic stiffness $\{c_{11}, c_{12}, c_{44}\}$ of superalloy CMSX-4 determined with Equation (2) at temperatures between 24 °C and 1300 °C are given in Table 2. The temperature dependencies of c_{ij} and other characteristics of elasticity are presented graphically in Figure 5. For simplicity, we will use the following notations: $E_{001} = E_{\langle 001 \rangle}$, $G_{001} = G_{\langle 001 \rangle \langle hk0 \rangle}$, and $\nu_{001} = \nu_{\langle 001 \rangle \langle hk0 \rangle}$ ($G_{\langle 001 \rangle \langle hk0 \rangle}$ and $\nu_{\langle 001 \rangle \langle hk0 \rangle}$ are independent of $\langle hk0 \rangle$).

Table 2. Temperature dependence of elastic stiffnesses c_{ij} of CMSX-4, GPa.

$T, ^\circ\text{C}$	24	200	400	600	800	1000	1100	1200	1250	1280	1300
c_{11}	250	243	236	227	218	199	193	189	186	185	185
c_{12}	161	158	155	152	150	141	144	149	152	154	156
c_{44}	129	123	117	110	102	93	87	79	74	70	69

It is seen from Figure 5a that the elastic moduli E_{001} and $G_{001} = c_{44}$ monotonically decrease with the temperature (elastic softening), which is a general trend for elastic solids. However, some elastic characteristics show a remarkable increase. Namely, the Zener factor of anisotropy A strongly increases with the temperature, from about 2.9 at RT to about 4.7 at 1300 °C, and Poisson's ratio ν_{001} respectively from about 0.39 to about 0.47. That is, ν_{001} approaches the maximum value of 0.5 possible at $\langle 001 \rangle$ orientation similar to that for elastically isotropic solids. This limitation follows from Equation (5) for the bulk modulus B in which the value becomes infinite at $\nu_{001} = 0.5$. This increase of ν_{001} with temperature results in a specific temperature change of B . In the temperature range RT–1000 °C, B decreases due to a decrease of E_{001} but at higher temperatures, it slightly increases due to an accelerated increase of ν_{001} .

$$B = \frac{E_{001}}{3(1 - 2\nu_{001})} \quad (5)$$

$$c_{11} = \frac{E_{001}(1 - \nu_{001})}{(1 + \nu_{001})(1 - 2\nu_{001})} \quad (6)$$

$$c_{12} = \frac{E_{001} \nu_{001}}{(1 + \nu_{001})(1 - 2 \nu_{001})} \quad (7)$$

The temperature changes of elastic stiffnesses c_{11} and c_{12} are also non-monotonous. From Table 2 and Figure 5 it follows that c_{11} decreases from 250 GPa at RT to 185 GPa at 1250 °C, but then remains constant. c_{12} changes similarly to B , by first decreasing from 161 GPa at RT to about 141 GPa at 1000 °C, but then increases to about 156 GPa at 1300 °C. The reason for the similar temperature dependencies of B , c_{11} , and c_{12} becomes clear from the comparison of their relationships with ν_{001} , see Equations (5)–(7). All these relationships include a divisor $(1 - 2 \nu_{001})$. Therefore, when ν_{001} approaches 0.5 the values of B and c_{12} increase, while c_{11} remains nearly constant.

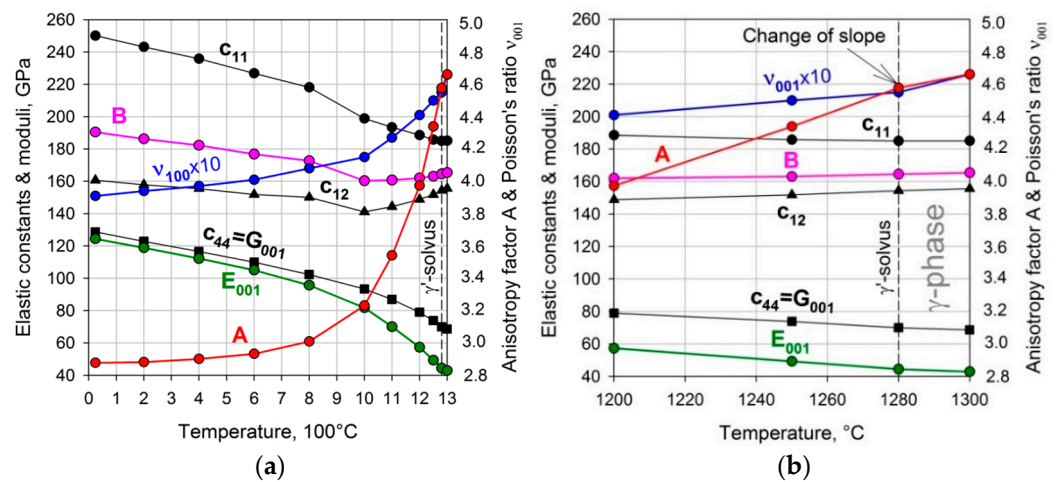


Figure 5. Temperature dependence of elastic stiffnesses $\{c_{11}, c_{12}, c_{44}\}$, Young, shear, and bulk moduli, respectively E_{001} , G_{001} , and B , Poisson's ratio ν_{001} , and Zener factor of elastic anisotropy A . (a) Is the presentation for the wide range 24–1300 °C and (b) gives an enlarged presentation for the vicinity of γ' -solvus temperature 1280 °C.

A remarkable feature of the measured temperature dependencies of elastic characteristics is that at the γ' -solvus temperature $T_s = 1280$ °C, most of them exhibit a change of slope, see Figure 5b. The reason for that is a transition from a two-phase state γ/γ' to a single γ -phase state. Therefore, the elastic constants measured at 1280 °C and above it, at 1300 °C, correspond to the γ -matrix of the superalloy CMSX-4. These results will be used below for an estimation of the elastic properties of γ - and γ' -phases.

For an analysis of the temperature dependence of the elastic properties of CMSX-4 and its analytical approximation, it is reasonable to select three independent elastic characteristics which monotonically change with a temperature up to T_s . The usually used elastic stiffnesses c_{ij} are obviously not suitable for this analysis because their temperature dependencies are non-monotonous, as mentioned above. However a good alternative for that are the elastic compliances s_{ij} related with c_{ij} by Equations (8)–(10):

$$s_{11} = \frac{c_{11} + c_{12}}{(c_{11} - c_{12})(c_{11} + 2c_{12})}, \quad (8)$$

$$s_{12} = -\frac{c_{12}}{(c_{11} - c_{12})(c_{11} + 2c_{12})}, \quad (9)$$

$$s_{44} = \frac{1}{c_{44}}. \quad (10)$$

Note that the Formulas (8) and (9) are invariant relative to $s_{ij} \leftrightarrow c_{ij}$ substitution. Figure 6a shows the temperature change of $\{s_{11}, s_{12}, s_{44}\}$ calculated with the data of Table 2 and Equations (8)–(10). It is seen that they monotonically increase in the temperature range

between RT and T_S . In this temperature interval, $s_{ij} = f(T)$ can be well fitted with a sum of linear and exponential functions of T , as defined by:

$$s_{ij} = a + b T + c \exp(d T), \quad (11)$$

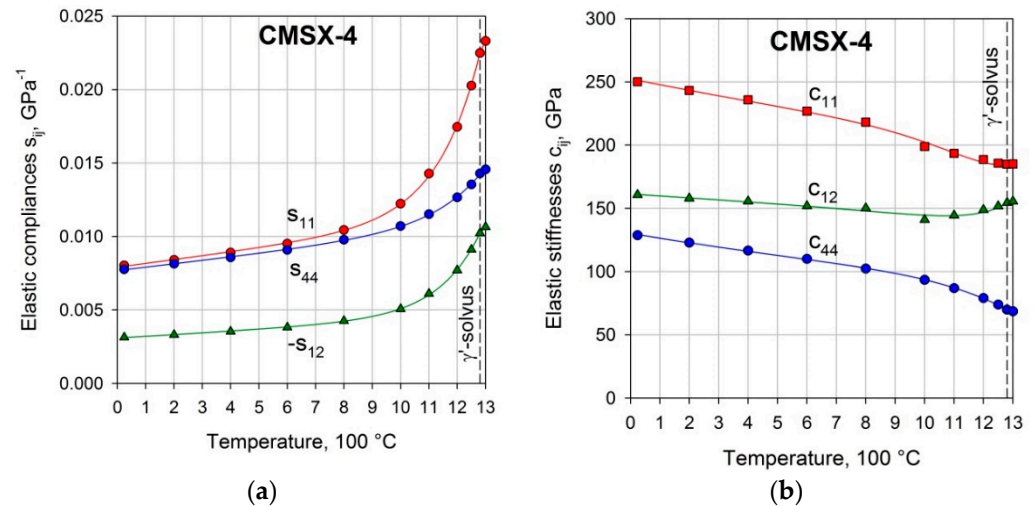


Figure 6. Elastic constants of superalloy CMSX-4 as functions of temperature. (a) Elastic compliances s_{ij} and (b) elastic stiffnesses c_{ij} . Symbols indicate the measured values, and the lines indicate the curves fitted with Equation (11).

The fitted parameters a , b , c , and d are given in Table 3.

Table 3. Fitted parameters of Equation (11) for CMSX-4.

Elastic Compliances of Superalloy CMSX-4				
s_{ij}, GPa^{-1}	$a, 10^{-3} \text{GPa}^{-1}$	$b, 10^{-6} \text{GPa}^{-1} \text{ }^\circ\text{C}^{-1}$	$c, 10^{-6} \text{GPa}^{-1}$	$d, 10^{-6} \text{ }^\circ\text{C}^{-1}$
s_{11}	7.90	2.58	2.10	6.71
$-s_{12}$	3.08	1.17	0.886	6.84
s_{44}	7.68	2.30	2.11	5.82

It is seen in Figure 6a that the temperature dependencies of elastic compliances $s_{ij} = f(T)$ of CMSX-4 are well fitted by Equation (11) and the approximating curves cross the experimental dots nearly in the middle. Taking the inverse version of Formulas (8)–(10) for the $s_{ij} \rightarrow c_{ij}$ conversion, the temperature dependencies of elastic stiffnesses $c_{ij} = f(T)$ were calculated, see Figure 6b. It is seen that the calculated curves $c_{ij}(T)$ correctly predict the temperature change of elastic stiffnesses as well.

3.2. Temperature Dependence of Elastic Constants of the Matrix Alloy

As was mentioned above, at the γ' -solvus temperature $1280\text{ }^\circ\text{C}$ and above, at $1300\text{ }^\circ\text{C}$, we actually measured the elastic properties of the γ -matrix of CMSX-4. Therefore, combining these results with those measured in [16] in the temperature range RT – $800\text{ }^\circ\text{C}$ for a γ -alloy compositionally similar to the matrix of CMSX-4, one can evaluate the elastic properties of γ -matrix over the entire temperature range. In order to fit these combined results, Equation (11) was used again, which showed high reliability when applied to CMSX-4. The fitted parameters a , b , c , and d for the matrix are given in Table 4.

Table 4. Fitted parameters of Equation (11) for the γ -matrix.

Elastic Compliances of Matrix				
$s_{ij}^m, \text{GPa}^{-1}$	$a, 10^{-3} \text{GPa}^{-1}$	$b, 10^{-6} \text{GPa}^{-1} \text{ } ^\circ\text{C}^{-1}$	$c, 10^{-6} \text{GPa}^{-1}$	$d, 10^{-6} \text{ } ^\circ\text{C}^{-1}$
s_{11}^m	7.49	4.44	1.05	7.10
$-s_{12}^m$	2.90	2.12	0.399	7.31
s_{44}^m	7.19	2.89	3.26	5.43

The fitted curves $s_{ij} = f(T)$ for the γ -matrix are shown in Figure 7a. It is seen that these curves have shapes similar to those for CMSX-4 (compare with Figure 6a) and pass through the experimental dots. The curves $c_{ij} = f(T)$ calculated from $s_{ij} = f(T)$ with inverse Equations (8)–(10) are plotted in Figure 7b. They have shapes that are also similar to those for CMSX-4 (compare with Figure 6b) and reasonably predict the experimental values of c_{ij} .

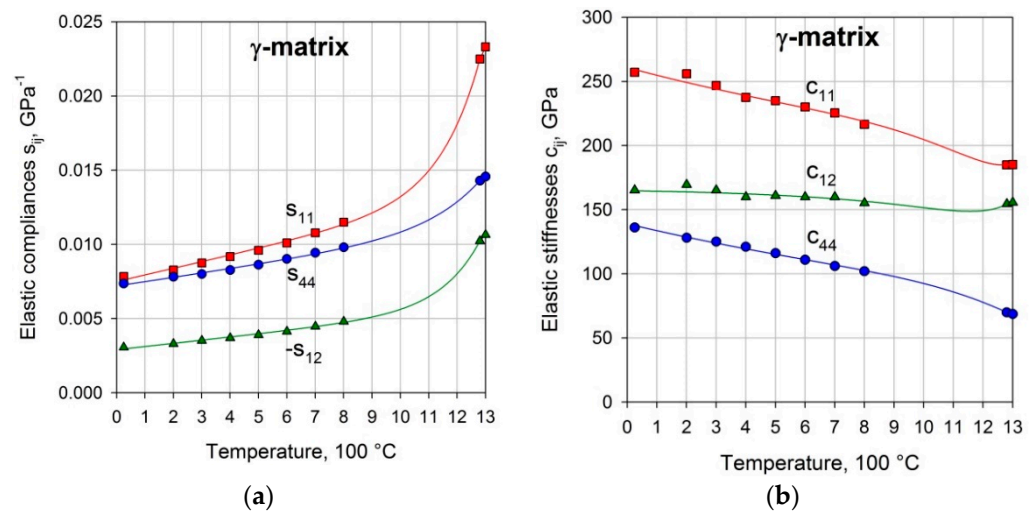


Figure 7. Elastic constants of the γ -matrix as functions of temperature. (a) Elastic compliances s_{ij} , and (b) elastic stiffnesses c_{ij} . Symbols indicate the measured values, and the lines indicate the curves fitted with Equation (11). The elastic constants of γ -matrix presented in the temperature range RT – $800 \text{ } ^\circ\text{C}$ were measured in [16].

3.3. Calculation of Elastic Constants for the γ' -Phase

The use of the bounds of Reuss (R) and Voigt (V) and their average as proposed by Hill (H) [52], provides a way to derive very simple estimates of the effective elastic properties of heterogeneous materials. For example, the RVH-rule of mixture was successfully applied in [31] to investigate contributions of the different phases to the effective Young's modulus of Ni-base superalloys. Even for textured polycrystals, the RVH was shown to provide estimates of the effective elastic stiffness that agree well with the self-consistent method with a much lower mathematical expenditure [53,54]. In this work, the RVH-rule of mixture is applied to the inverse problem, namely for the estimation of the elastic properties of the constituent phase γ' using the elastic properties measured for the superalloy (γ/γ' -compound) and its γ -matrix (another constituent phase). The applied procedure, which is based on the RVH-rule of mixture, is described below. It is worth mentioning that misfit (coherency) stresses have no influence on the effective elastic constants of the compound due to the principle of superposition in linear elasticity (see, e.g., [55]).

If $\mathbf{C}(x)$ and $\mathbf{S}(x)$ respectively denote the local stiffness and compliance tensors, and \mathbf{C}^{eff} and \mathbf{S}^{eff} denote the effective stiffness and compliance tensors, the bounds of Voigt

and Reuss are based on the following inequalities of quadratic forms specifying the elastic energy functional, as derived by Hill [56]:

$$\mathbf{E} : \mathbf{C}^{\text{eff}} : \mathbf{E} \leq \mathbf{E} : \langle \mathbf{C} \rangle : \mathbf{E}, \quad (12)$$

$$\mathbf{\Sigma} : \mathbf{S}^{\text{eff}} : \mathbf{\Sigma} \leq \mathbf{\Sigma} : \langle \mathbf{S} \rangle : \mathbf{\Sigma}, \quad (13)$$

where \mathbf{E} and $\mathbf{\Sigma}$ are respectively arbitrary strain and stress tensors. Here, and in the following of this section, the notation $\langle x \rangle$ represents the volume average of the quantity x in a representative volume.

A rigorous way to obtain bounds of the effective elastic properties of a compound is to use the spectral decomposition of the tensors of elastic stiffness and compliance, which in the case of cubic symmetry is given by:

$$\mathbf{C} = \sum_{i=1}^3 \lambda_i \mathbf{P}_i, \quad (14)$$

$$\mathbf{S} = \mathbf{C}^{-1} = \sum_{i=1}^3 \lambda_i^{-1} \mathbf{P}_i, \quad (15)$$

where \mathbf{P}_i are three orthogonal fourth order basis tensors such that $\mathbf{P}_i : \mathbf{P}_j = 0$ if $i \neq j$, $\mathbf{P}_i : \mathbf{P}_i = \mathbf{P}_i$, and $\mathbf{P}_i :: \mathbf{P}_j = \delta_{ij}$, and λ_i are three eigenvalues of the tensor \mathbf{C} . This decomposition of the elasticity stiffness tensor in orthonormal modes can be traced back to the historic work of Lord Kelvin [57]. For a more recent presentation, one can consult the references [58–60]. The Voigt's representation of the basis tensors is:

$$\mathbf{P}_1^{\text{V}} = \frac{1}{3} \begin{bmatrix} 1 & 1 & 1 & 0 & 0 & 0 \\ 1 & 1 & 1 & 0 & 0 & 0 \\ 1 & 1 & 1 & 0 & 0 & 0 \\ 0 & 0 & 0 & 0 & 0 & 0 \\ 0 & 0 & 0 & 0 & 0 & 0 \\ 0 & 0 & 0 & 0 & 0 & 0 \end{bmatrix} \quad (16)$$

$$\mathbf{P}_2^{\text{V}} = \frac{1}{3} \begin{bmatrix} 2 & -1 & -1 & 0 & 0 & 0 \\ -1 & 2 & -1 & 0 & 0 & 0 \\ -1 & -1 & 2 & 0 & 0 & 0 \\ 0 & 0 & 0 & 0 & 0 & 0 \\ 0 & 0 & 0 & 0 & 0 & 0 \\ 0 & 0 & 0 & 0 & 0 & 0 \end{bmatrix} \quad (17)$$

$$\mathbf{P}_3^{\text{V}} = \frac{1}{2} \begin{bmatrix} 0 & 0 & 0 & 0 & 0 & 0 \\ 0 & 0 & 0 & 0 & 0 & 0 \\ 0 & 0 & 0 & 0 & 0 & 0 \\ 0 & 0 & 0 & 1 & 0 & 0 \\ 0 & 0 & 0 & 0 & 1 & 0 \\ 0 & 0 & 0 & 0 & 0 & 1 \end{bmatrix} \quad (18)$$

The eigenvalues λ_i following from the system of linear equations defined by Equations (14), (16)–(18) are:

$$\lambda_1 = c_{11} + 2 c_{12}, \quad (19)$$

$$\lambda_2 = c_{11} - c_{12}, \quad (20)$$

$$\lambda_3 = 2 c_{44}. \quad (21)$$

The inverse conversion $\lambda_i \rightarrow c_{ij}$ is defined by:

$$c_{11} = (\lambda_1 + 2\lambda_2)/3, \quad (22)$$

$$c_{12} = (\lambda_1 - \lambda_2)/3, \quad (23)$$

$$c_{44} = \lambda_3/2. \quad (24)$$

For a nickel-base superalloy with a composite γ/γ' -microstructure, the spectral decomposition (14) can be separately applied to the stiffness tensors of a γ/γ' -compound and each phase, γ and γ' , respectively to \mathbf{C}^{eff} , \mathbf{C}^{m} , and \mathbf{C}^{P} :

$$\mathbf{C}^{\text{eff}} = \sum_{i=1}^3 \lambda_i^{\text{eff}} \mathbf{P}_i, \quad (25)$$

$$\mathbf{C}^{\text{m}} = \sum_{i=1}^3 \lambda_i^{\text{m}} \mathbf{P}_i, \quad (26)$$

$$\mathbf{C}^{\text{P}} = \sum_{i=1}^3 \lambda_i^{\text{P}} \mathbf{P}_i, \quad (27)$$

which results in three sets of the eigenvalues: λ_i^{eff} for the γ/γ' -compound, and λ_i^{m} and λ_i^{P} for the constitutive γ - and γ' -phases. Due to Equation (15), the corresponding decompositions hold for the compliance tensors \mathbf{S}^{eff} , \mathbf{S}^{m} , and \mathbf{S}^{P} . A consequence of the spectral decomposition (14,15) is that the inequalities (12,13) can be rewritten in the following form:

$$\sum_{i=1}^3 \lambda_i^{\text{eff}} \mathbf{E}_i : \mathbf{P}_i : \mathbf{E}_i \leq \sum_{i=1}^3 \langle \lambda_i \rangle \mathbf{E}_i : \mathbf{P}_i : \mathbf{E}_i \quad (28)$$

$$\sum_{i=1}^3 \left(\lambda_i^{\text{eff}} \right)^{-1} \boldsymbol{\Sigma}_i : \mathbf{P}_i : \boldsymbol{\Sigma}_i \leq \sum_{i=1}^3 \langle \lambda_i^{-1} \rangle \boldsymbol{\Sigma}_i : \mathbf{P}_i : \boldsymbol{\Sigma}_i, \quad (29)$$

where \mathbf{E}_1 , \mathbf{E}_2 , and \mathbf{E}_3 are three orthogonal eigentensors of \mathbf{C} corresponding to three deformation eigenmodes, that is, dilatation, deviatoric tetragonal distortion in the crystal axes, and pure shear. These deformation eigenmodes \mathbf{E}_i are respectively related by the elasticity law to the three orthogonal stress tensors $\boldsymbol{\Sigma}_i$, where $\boldsymbol{\Sigma}_1$ is a hydrostatic stress tensor, and $\boldsymbol{\Sigma}_2$ and $\boldsymbol{\Sigma}_3$ two deviatoric stress tensors.

As the three tensors \mathbf{E}_i as well as $\boldsymbol{\Sigma}_i$ are independent, and the inequalities (28) and (29) are valid for any \mathbf{E}_i and $\boldsymbol{\Sigma}_i$, the following inequalities hold:

$$\lambda_i^{\text{eff}} \leq \langle \lambda_i \rangle \quad (30)$$

$$\left(\lambda_i^{\text{eff}} \right)^{-1} \leq \langle \lambda_i^{-1} \rangle. \quad (31)$$

Combining (30) and (31) gives the lower Reuss and upper Voigt bonds for λ_i^{eff} :

$$\lambda_i^{\text{R}} = \langle \lambda_i^{-1} \rangle^{-1} \leq \lambda_i^{\text{eff}} \leq \lambda_i^{\text{V}} = \langle \lambda_i \rangle, \quad (32)$$

which correspond to the serial and parallel arrangement of constituents and are given by:

$$\lambda_i^{\text{R}} = \left[(1 - f^{\text{P}}) (\lambda_i^{\text{m}})^{-1} + f^{\text{P}} (\lambda_i^{\text{P}})^{-1} \right]^{-1}, \quad (33)$$

$$\lambda_i^{\text{V}} = (1 - f^{\text{P}}) \lambda_i^{\text{m}} + f^{\text{P}} \lambda_i^{\text{P}}, \quad (34)$$

where f^{P} is the γ' -volume fraction.

Thus, an estimate of the effective properties can be obtained by the arithmetic average of the bounds $\lambda_i^{\text{eff},1} = 1/2(\lambda_i^{\text{R}} + \lambda_i^{\text{V}})$ or alternatively by harmonic average $1/\lambda_i^{\text{eff},2} = 1/2(1/\lambda_i^{\text{R}} + 1/\lambda_i^{\text{V}})$. However, a theoretical drawback of these averages is their lack of

consistency, because $\lambda_i^{\text{eff},1} \neq \lambda_i^{\text{eff},2}$. As mentioned earlier by Hill [52], a more consistent estimate is the geometric average:

$$\lambda_i^{\text{eff}} = \sqrt{\lambda_i^{\text{R}} \lambda_i^{\text{V}}}, \quad (35)$$

which removes this inconsistency (see, e.g., [61]).

The elastic constants of the γ' -phase can be estimated using Equation (35) by setting the effective constants to those determined for CMSX-4, that is $\lambda_i^{\text{eff}} = \lambda_i^{\text{a}}$ (the superscript “a” means alloy CMSX-4) and solving with respect to λ_i^{p} the Equations:

$$\lambda_i^{\text{a}} = \sqrt{\lambda_i^{\text{R}}(\lambda_i^{\text{m}}, \lambda_i^{\text{p}}) \lambda_i^{\text{V}}(\lambda_i^{\text{m}}, \lambda_i^{\text{p}})}, \quad (36)$$

where $\lambda_i^{\text{R}}(\lambda_i^{\text{m}}, \lambda_i^{\text{p}})$ and $\lambda_i^{\text{V}}(\lambda_i^{\text{m}}, \lambda_i^{\text{p}})$ are given by Equations (33) and (34). After some rearrangement, the last Equation can be transformed in a quadratic equation for the unknown λ_i^{p} , which has only one positive root. Finally, with the substitution $\xi_i = \lambda_i^{\text{a}} / \lambda_i^{\text{m}}$, this solution can be written as:

$$\lambda_i^{\text{p}} = \frac{\lambda_i^{\text{m}}}{2} \left[-\left(\frac{1-f^{\text{p}}}{f^{\text{p}}}\right) (1 - \xi_i^2) + \sqrt{\left(\frac{1-f^{\text{p}}}{f^{\text{p}}}\right)^2 (1 - \xi_i^2)^2 + 4 \xi_i^2} \right] \quad (37)$$

Summing up the above analytical computation, one can define the following steps for calculating the elastic stiffnesses c_{ij}^{p} of the γ' -phase:

1. Using c_{ij}^{a} and c_{ij}^{m} defined by Equation (11) with $\{a, b, c, d\}$ given in Tables 3 and 4, calculate λ_i^{a} and λ_i^{m} by Equations (19)–(21);
2. With the substitution $\xi_i = \lambda_i^{\text{a}} / \lambda_i^{\text{m}}$ and f^{p} defined by Equation (4), calculate λ_i^{p} by Equation (37);
3. Using λ_i^{p} , calculate c_{ij}^{p} by Equations (22)–(24).

It should be mentioned that at temperatures close to the γ' -solvus temperature $T_S = 1280$ °C, the γ' -fraction f^{p} approaches zero and accordingly the term $(1 - f^{\text{p}}) / f^{\text{p}}$ in Equation (37) takes too high values, which leads to wrong results. Therefore, in this work c_{ij}^{p} were calculated for temperatures up to 1250 °C, which was the highest temperature in the f^{p} -measurements.

Figure 8 shows together the temperature dependencies of elastic stiffnesses of alloy CMSX-4 and its phases γ and γ' , respectively c_{ij}^{a} , c_{ij}^{m} , and c_{ij}^{p} . It is seen that the curves $c_{ij}^{\text{a}}(T)$, $c_{ij}^{\text{m}}(T)$, and $c_{ij}^{\text{p}}(T)$ have similar shapes and the values of c_{ij}^{a} , c_{ij}^{m} , and c_{ij}^{p} are quite close. At all relevant temperatures, the inequalities $c_{11}^{\text{m}}(T) > c_{11}^{\text{a}}(T) > c_{11}^{\text{p}}(T)$ and $c_{12}^{\text{m}}(T) > c_{12}^{\text{a}}(T) > c_{12}^{\text{p}}(T)$ apply. For c_{44} , the same inequality is valid up to a temperature of about 800 °C but at higher temperatures, the c_{44} values of CMSX-4 and its phases become very close, $c_{44}^{\text{m}}(T) \approx c_{44}^{\text{a}}(T) \approx c_{44}^{\text{p}}(T)$.

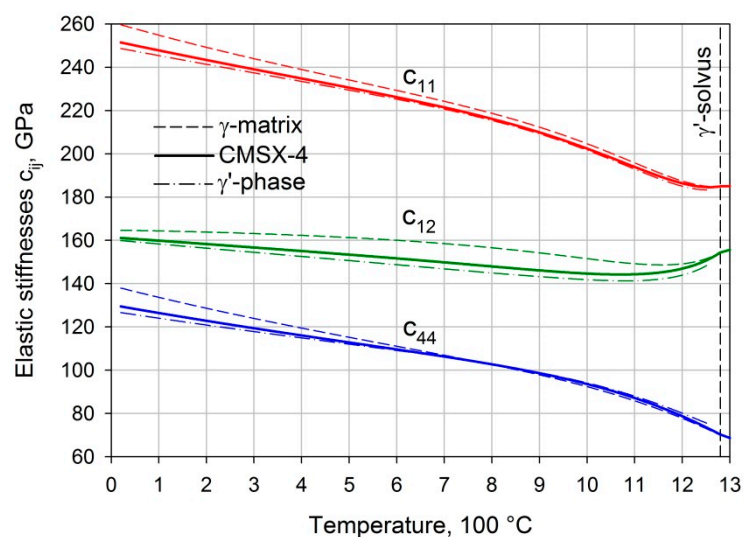


Figure 8. Temperature dependences of the elastic stiffnesses c_{ij} of CMSX-4, its γ -matrix and γ' -phase.

4. Discussion

The elastic constants of single-crystal nickel-base superalloy CMSX-4 were measured by the sonic resonance method in a wide temperature interval between room temperature and 1300 °C. The accuracy of such a measurement is influenced by many factors and consequently the total measurement error can be quite large. Therefore, in order to achieve a high measurement accuracy, a negative effect of every factor has to be minimized.

For example, the effect of a change of the material density with a temperature can be discussed. The general relationship between the elastic moduli M (E or G) measured by the resonance method, the specimen parameters and the resonance frequency f_R is given by:

$$M = K_S \rho f_R^2, \quad (38)$$

where K_S is the factor of specimen geometry and ρ is the material density. It follows from Figure 3 that an increase of temperature from RT to 1300 °C results in the thermal expansion of CMSX-4 by about 2.5%, which according to the relationship $\rho(T) = \rho(RT)/[1 + \varepsilon_T(T)]^3$, corresponds to a decrease of material density by about 7.7%. Thus, neglecting the temperature expansion $\varepsilon_T(T)$, that is assuming $\rho(T) \approx \rho(RT)$, results in the same error of the measured elastic moduli. Therefore, in this work the thermal expansion of CMSX-4 investigated over an entire temperature interval as well as the alloy density at room temperature $\rho(RT)$ was precisely measured.

Single-crystals of nickel-base superalloys are characterized by high elastic anisotropy which significantly increases with temperatures. As mentioned above, the Zener factor of anisotropy A of CMSX-4 increases from about 2.9 at RT to about 4.7 at 1300 °C. Therefore, for a reliable characterization of the elastic properties of such strongly anisotropic materials, it is important to investigate many specimens of different crystallographic orientations, as well as to excite different vibration modes. This was done in the present investigation.

A decisive point of the whole investigation is the determination of the elastic constants by computing the resonance frequencies. Here the specimen geometry and its exact crystallographic orientation have to be accurately considered. This cannot be done in analytical approaches, which assume ideal orientations with high symmetries. In contrast, this can be realized by finite element method, as it was computed in this work.

The resonance measurements performed at super-solvus temperatures allowed us to determine the elastic constants of the γ -matrix of CMSX-4 in the temperature interval 1280–1300 °C. Combining the results of this work obtained with the results reported by Siebörger et al. [16] for an alloy compositionally similar to the matrix of CMSX-4, the elastic constants of the γ -matrix c_{ij}^m over an entire temperature range were estimated. Precisely

measuring the temperature change of the γ' -fraction f^P and applying the Reuss–Voigt–Hill rule of mixture, the elastic constants of the γ' -phase c_{ij}^P were estimated as well. The obtained values of c_{ij}^m and c_{ij}^P can be used for advanced physically-based modeling of the mechanical behavior of nickel-base superalloys explicitly considering the γ/γ' -microstructure.

Besides this, the obtained values of c_{ij}^m and c_{ij}^P can be applied for the verification of Nabarro's elastic concept for rafting. Figure 9 shows the predicted temperature dependence of the misfit m of the elastic moduli $M^m = c_{11}^m - c_{12}^m$ and $M^P = c_{11}^P - c_{12}^P$, as defined by Equation (1). It is seen that at temperatures where the γ' -rafting is usually observed, 900–1150 °C, the value of m for superalloy CMSX-4 is positive. It is known [37,62], that the lattice misfit of CMSX-4 is negative, $\delta < 0$. Thus, the term $\delta \times m$ is negative too. This fits with Nabarro's elastic concept for rafting, predicting N-rafting under tensile $\langle 001 \rangle$ loading when $\delta \times m < 0$. It is remarkable that the curve $m(T)$ predicted for CMSX-4 in this work passes through the middle of scattering area of literature data reported for m in different Ni-base alloys. This agreement with the literature data testifies the reliability of results obtained in this work.

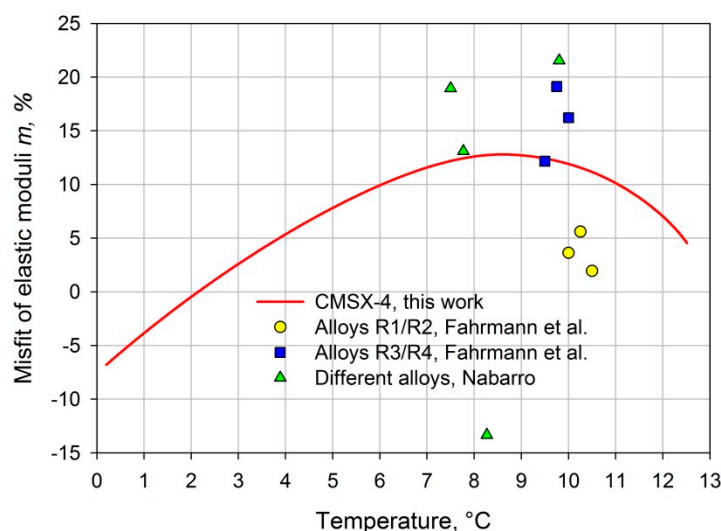


Figure 9. Temperature dependence of the misfit m of elastic moduli $M^m = c_{11}^m - c_{12}^m$ and $M^P = c_{11}^P - c_{12}^P$. The solid line is $m = f(T)$ determined for CMSX-4 in this work, the symbols are data from Fahrman et al. [32] and Nabarro [25].

5. Conclusions

1. The elastic constants of single-crystal nickel-base superalloy CMSX-4 were precisely measured by the sonic resonance method at temperatures between room temperature and 1300 °C. This wide temperature interval covered all areas where the elastic constants of CMSX-4 are needed, namely: Service conditions of the blade material, technical accidents of gas turbines (overheating), as well as the manufacturing of turbine blades (hot isostatic pressing and heat treatment);

2. Combining the results of this work obtained for superalloy CMSX-4 with the results reported by Siebörger et al. [16] for an alloy similar to the γ -matrix of CMSX-4 and applying the Reuss–Voigt–Hill rule of mixture, the elastic constants of the γ - and γ' -phases, c_{ij}^m and c_{ij}^P , were estimated in the temperature range between room temperature and 1250 °C. The obtained values of c_{ij}^m and c_{ij}^P could be used for advanced physically-based modeling of the mechanical behavior of nickel-base superalloys explicitly considering the γ/γ' -microstructure;

3. The estimated elastic constants c_{ij}^m and c_{ij}^P were used to predict the temperature dependence of the misfit m of elastic moduli $M^m = c_{11}^m - c_{12}^m$ and $M^P = c_{11}^P - c_{12}^P$. It was shown that at temperatures where the γ' -rafting occurs, 900–1150 °C, the value of m for superalloy CMSX-4 was positive, $m > 0$. Since CMSX-4 is an alloy with a negative lattice

misfit, $\delta < 0$, such a result for the sign of m fits with Nabarro's elastic concept for rafting predicting N-rafting under tensile $\langle 001 \rangle$ loading when $\delta \times m < 0$.

Author Contributions: Conceptualization and methodology, A.E. and B.F.; formal analysis, G.K.; investigation, M.F., B.R. and C.L.; resources, N.P. and I.S.; writing—original draft preparation, A.E. and B.F.; project administration, G.N. All authors have read and agreed to the published version of the manuscript.

Funding: This research was funded by the Deutsche Forschungsgemeinschaft (grants RE 688/77-1 and NO 307/9-1) and the Russian Foundation of Basic Research (grant 18-508-12010).

Institutional Review Board Statement: Not applicable.

Informed Consent Statement: Not applicable.

Data Availability Statement: Additional data can be provided by simple request via Email to B.F.

Acknowledgments: Authors are grateful to U. Glatzel, University of Bayreuth for supplying the numerical data for the elastic properties of the γ -matrix of CMSX-4.

Conflicts of Interest: The authors declare no conflict of interest.

Appendix A

Table A1. Thermal expansion of CMSX-4 as a function of temperature, $\varepsilon_T = f(T)$, in %. Rows in -100°C intervals, and columns in -10°C intervals.

$T, ^\circ\text{C}$	0	10	20	30	40	50	60	70	80	90
0			0	-	-	0.0238	0.0329	0.0425	0.053	0.0641
100	0.076	0.088	0.1	0.113	0.125	0.138	0.15	0.16	0.176	0.19
200	0.203	0.217	0.23	0.245	0.258	0.272	0.286	0.3	0.314	0.329
300	0.342	0.355	0.368	0.382	0.396	0.41	0.424	0.438	0.451	0.464
400	0.479	0.494	0.508	0.523	0.537	0.552	0.567	0.581	0.596	0.61
500	0.625	0.639	0.653	0.667	0.682	0.697	0.712	0.727	0.743	0.758
600	0.774	0.79	0.806	0.822	0.839	0.856	0.873	0.89	0.906	0.924
700	0.941	0.958	0.975	0.993	1.01	1.03	1.05	1.06	1.08	1.1
800	1.12	1.14	1.15	1.17	1.19	1.21	1.23	1.25	1.27	1.29
900	1.31	1.33	1.35	1.38	1.4	1.42	1.44	1.46	1.49	1.51
1000	1.53	1.56	1.58	1.61	1.63	1.66	1.68	1.71	1.74	1.76
1100	1.79	1.82	1.85	1.88	1.91	1.94	1.97	2.01	2.04	2.07
1200	2.11	2.15	2.18	2.22	2.26	2.3	2.35	2.39	2.44	2.47
1300	2.5	2.52								

References

1. Reed, R.C. *The Superalloys: Fundamentals and Applications*; Cambridge University Press: Cambridge, UK, 2006. [CrossRef]
2. Shalin, R.E.; Svetlov, I.L.; Kachanov, E.B.; Toloraya, V.N.; Gavrilin, O.S. *Single-Crystals of Nickel-Base Superalloys*; Mashinostroeniye: Moscow, Russia, 1997.
3. Ghosh, R.N.; Curtis, R.V.; McLean, M. Creep deformation of single crystal superalloys—Modelling the crystallographic anisotropy. *Acta Metall. Mater.* **1990**, *38*, 1977–1992. [CrossRef]
4. Méric, L.; Poubanne, P.; Cailletaud, G. Single Crystal Modeling for Structural Calculations: Part 1—Model Presentation. *J. Eng. Mater. Technol.* **1991**, *113*, 162–170. [CrossRef]
5. Meéric, L.; Cailletaud, G. Single Crystal Modeling for Structural Calculations: Part 2—Finite Element Implementation. *J. Eng. Mater. Technol.* **1991**, *113*, 171–182. [CrossRef]
6. Tinga, T. Multiscale Modelling of Single Crystal Superalloys for Gas Turbine Blades. Ph.D. Thesis, Eindhoven University of Technology, Eindhoven, The Netherlands, 7 May 2009. [CrossRef]
7. Zhou, N.; Shen, C.; Mills, M.; Wang, Y. Contributions from elastic inhomogeneity and from plasticity to γ' rafting in single-crystal Ni–Al. *Acta Mater.* **2008**, *56*, 6156–6173. [CrossRef]
8. Link, T.; Epishin, A.; Fedelich, B. Inhomogeneity of misfit stresses in nickel-base superalloys: Effect on propagation of matrix dislocation loops. *Philos. Mag.* **2009**, *89*, 1141–1159. [CrossRef]
9. Cottura, M.; Appolaire, B.; Finel, A.; Le Bouar, Y. Coupling the Phase Field Method for diffusive transformations with dislocation density-based crystal plasticity: Application to Ni-based superalloys. *J. Mech. Phys. Solids* **2016**, *94*, 473–489. [CrossRef]

10. Böttger, B.; Apel, M.; Budnitski, M.; Eiken, J.; Laschet, G.; Zhou, B. Calphad coupled phase-field model with mechano-chemical contributions and its application to rafting of γ' in CMSX-4. *Comput. Mater. Sci.* **2020**, *184*, 109909. [CrossRef]
11. Krivko, A.I.; Epishin, A.I.; Svetlov, I.L.; Samoilov, A.I. Elastic properties of single crystals of nickel alloys. *Strength Mater.* **1988**, *20*, 214–223. [CrossRef]
12. Svetlov, I.L.; Epishin, A.I.; Krivko, A.I.; Samoilov, A.I.; Odintsev, I.N.; Andreev, A.P. Anisotropy of Poisson ratio of nickel-base alloy single-crystals. *Dokl. Akad. Nauk SSSR* **1988**, *302*, 1372–1375.
13. Epishin, A.I.; Lisovenko, D.S. Extreme values of the Poisson's ratio of cubic crystals. *Tech. Phys.* **2016**, *61*, 1516–1524. [CrossRef]
14. Schneider, W. Hochtemperaturkriechverhalten und Mikrostruktur der einkristallinen Nickelbasis-Superlegierung CMSX-4 bei Temperaturen von 800 °C bis 1100 °C. Ph.D. Thesis, University of Erlangen-Nuremberg, Erlangen-Nuremberg, Germany, 1993.
15. Hermann, W.; Sockel, H.; Han, J.; Bertram, A. Elastic properties and determination of elastic constants of nickel-base superalloys by a free-free beam technique. In Proceedings of the Superalloys 1996, Seven Springs Mountain Resort, Champion, PA, USA, 22–26 September 1996; Kissinger, R.D., Deye, D.J., Anton, D.L., Cetel, A.D., Nathal, M.V., Pollock, T.M., Woodford, D.A., Eds.; TMS: Warrendale, PA, USA, 2000; pp. 229–238. [CrossRef]
16. Siebörger, D.; Knake, H.; Glatzel, U. Temperature dependence of the elastic moduli of the nickel-base superalloy CMSX-4 and its isolated phases. *Mater. Sci. Eng. A* **2001**, *298*, 26–33. [CrossRef]
17. Demtröder, K.; Eggeler, G.; Schreuer, J. Influence of microstructure on macroscopic elastic properties and thermal expansion of nickel-base superalloys ERBO/1 and LEK94. *Mater. Werkst.* **2015**, *46*, 563–576. [CrossRef]
18. Le Graverend, J.-B.; Cormier, J.; Gallerneau, F.; Kruch, S.; A Mendez, J. Highly non-linear creep life induced by a short close γ' -solvus overheating and a prior microstructure degradation on a nickel-based single crystal superalloy. *Mater. Des.* **2014**, *56*, 990–997. [CrossRef]
19. Epishin, A.; Fedelich, B.; Link, T.; Feldmann, T.; Svetlov, I.L. Pore annihilation in a single-crystal nickel-base superalloy during hot isostatic pressing: Experiment and modelling. *Mater. Sci. Eng. A* **2013**, *586*, 342–349. [CrossRef]
20. Epishin, A.; Link, T.; Fedelich, B.; Svetlov, I.L.; Golubovskiy, E.R. Hot isostatic pressing of single-crystal nickel-base superalloys: Mechanism of pore closure and effect on mechanical properties. In Proceedings of the Eurosuperalloys 2014, Giens, France, 12–16 May 2014; Guedou, J.Y., Ed.; EDP: Les Ulis, France, 2014; Volume 14, p. 8003. [CrossRef]
21. Epishin, A.; Fedelich, B.; Nolze, G.; Schriever, S.; Feldmann, T.; Ijaz, M.F.; Viguier, B.; Poquillon, D.; Le Bouar, Y.; Ruffini, A.; et al. Creep of Single Crystals of Nickel-Based Superalloys at Ultra-High Homologous Temperature. *Met. Mater. Trans. A* **2018**, *49*, 3973–3987. [CrossRef]
22. Tien, J.K.; Copley, S.M. The effect of uniaxial stress on the periodic morphology of coherent gamma prime precipitates in nickel-base superalloy crystals. *Met. Mater. Trans. A* **1971**, *2*, 215–219. [CrossRef]
23. Pineau, A. Influence of uniaxial stress on the morphology of coherent precipitates during coarsening-elastic energy considerations. *Acta Met.* **1976**, *24*, 559–564. [CrossRef]
24. Svetlov, I.; Golovko, B.; Epishin, A.; Abalakin, N. Diffusional mechanism of γ' -phase particles coalescence in single crystals of nickel-base superalloys. *Scr. Met. Mater.* **1992**, *26*, 1353–1358. [CrossRef]
25. Nabarro, F.R.N. Rafting in Superalloys. *Met. Mater. Trans. A* **1996**, *27*, 513–530. [CrossRef]
26. Nazmy, M.; Epishin, A.; Link, T.; Stäubli, M. A review of degradation in single crystal nickel based superalloys. *Energy Mater.* **2006**, *1*, 263–268. [CrossRef]
27. Fedelich, B.; Epishin, A.; Link, T.; Klingelhöffer, H.; Künecke, G.; Portella, P.D. Rafting during high temperature deformation in a single crystal superalloy: Experiments and modeling. In Proceedings of the Superalloys 2012, Seven Springs Mountain Resort, Champion, PA, USA, 9–13 September 2012; Huron, E.S., Reed, R.C., Hardy, M.C., Mills, M.J., Montero, R.E., Portella, P.D., Telesman, J., Eds.; TMS: Warrendale, PA, USA, 2012; pp. 491–500. Available online: https://www.tms.org/Superalloys/10.7449/2012/Superalloys_2012_491_500.pdf (accessed on 1 October 2020).
28. Titus, M.S.; Suzuki, A.; Pollock, T.M. High Temperature creep of new L12 containing cobalt-base superalloys. In Proceedings of the Superalloys 2012, Seven Springs Mountain Resort, Champion, PA, USA, 9–13 September 2012; Huron, E.S., Reed, R.C., Hardy, M.C., Mills, M.J., Montero, R.E., Portella, P.D., Telesman, J., Eds.; TMS: Warrendale, PA, USA, 2012; pp. 823–832. Available online: https://www.tms.org/Superalloys/10.7449/2012/Superalloys_2012_823_832.pdf (accessed on 1 October 2020).
29. Epishin, A.; Petrushin, N.; Nolze, G.; Gerstein, G.; Maier, H.J. Investigation of the γ' -Strengthened Quaternary Co-Based Alloys Co-Al-W-Ta. *Met. Mater. Trans. A* **2018**, *49*, 4042–4057. [CrossRef]
30. Fisher, E. On the elastic moduli of nickel rich Ni-Al alloy single crystals. *Scr. Met.* **1986**, *20*, 279–284. [CrossRef]
31. Kuhn, H.-A.; Sockel, H.G. Contributions of the Different Phases of Two Nickel-Base Superalloys to the Elastic Behaviour in a Wide Temperature Range. *Phys. Status Solidi* **1990**, *119*, 93–105. [CrossRef]
32. Fahrman, M.; Hermann, W.; Boegli, A.; Pollock, T.; Sockel, H. Determination of matrix and precipitate elastic constants in (γ - γ') Ni-base model alloys, and their relevance to rafting. *Mater. Sci. Eng. A* **1999**, *260*, 212–221. [CrossRef]
33. Ichitsubo, T.; Koumoto, D.; Hirao, M.; Tanaka, K.; Osawa, M.; Yokokawa, T.; Harada, H. Elastic anisotropy of rafted Ni-base superalloy at high temperatures. *Acta Mater.* **2003**, *51*, 4863–4869. [CrossRef]
34. Dye, D.; Coakley, J.; Vorontsov, V.A.; Stone, H.J.; Rogge, R. Elastic moduli and load partitioning in a single-crystal nickel superalloy. *Scr. Mater.* **2009**, *61*, 109–112. [CrossRef]

35. Harris, K.; Erickson, G.L.; Sikkenga, S.L.; Brentnall, W.D.; Aurrecochea, J.M.; Kubarych, K.G. Development of two rhenium containing superalloys for single crystal blade and directionally solidified vane applications in advanced turbine engines. *J. Mater. Eng. Perform.* **1993**, *2*, 481–487. [[CrossRef](#)]
36. Brückner, U.; Epishin, A.; Link, T. Local X-ray diffraction analysis of the structure of dendrites in single-crystal nickel-base superalloys. *Acta Mater.* **1997**, *45*, 5223–5231. [[CrossRef](#)]
37. Brückner, U.; Epishin, A.; Link, T.; Dressel, K. The influence of the dendritic structure on the γ/γ' -lattice misfit in the single-crystal nickel-base superalloy CMSX-4. *Mater. Sci. Eng. A* **1998**, *247*, 23–31. [[CrossRef](#)]
38. Förster, F. Ein neues Messverfahren zur Bestimmung des Elastizitätsmoduls und der Dämpfung. *Z. Metallkunde* **1937**, *29*, 109–115.
39. ASTM International. Standard Test Method for Dynamic Young's Modulus, Shear Modulus, and Poisson's Ratio by Sonic Resonance. Revision 13. ASTM E1875. Available online: <https://www.astm.org/Standards/E1875.htm> (accessed on 1 December 2020).
40. Zienkiewicz, O.C.; Taylor, R.L. *The Finite Element Method*, 5th ed.; Butterworth & Heinemann: Oxford, UK, 2000; Volume 1.
41. Abaqus/Standard. 3ds.com. Available online: <https://www.3ds.com/products-services/simulia/products/abaqus/abaqusstandard/> (accessed on 1 February 2021).
42. Link, T.; Epishin, A.; Gottwald, A.; Wichmann, T. Quantitative analysis of the structure of single crystal superalloys. In Proceedings of the Fortschritte in der Metallographie, 37 Metallographie-Tagung, Berlin, Germany, 17–19 September 2003; Portella, P.D., Ed.; Werkstoff-Informationsges: Frankfurt, Germany, 2004; pp. 257–262.
43. Cormier, J.; Milhet, X.; Mendez, J. Effect of very high temperature short exposures on the dissolution of the γ' phase in single crystal MC2 superalloy. *J. Mater. Sci.* **2007**, *42*, 7780–7786. [[CrossRef](#)]
44. Tiley, J.; Viswanathan, G.; Hwang, J.; Shiveley, A.; Banerjee, R. Evaluation of gamma prime volume fractions and lattice misfits in a nickel base superalloy using the external standard X-ray diffraction method. *Mater. Sci. Eng. A* **2010**, *528*, 32–36. [[CrossRef](#)]
45. Glatzel, U. *Microstructure and Internal Strains of Undeformed and Creep Deformed Samples of a Nickel-Base Superalloy*; Verlag Dr. Köster: Berlin, Germany, 1994.
46. Hemmersmeier, U.; Feller-Kniepmeier, M. Element distribution in the macro- and microstructure of nickel base superalloy CMSX-4. *Mater. Sci. Eng. A* **1998**, *248*, 87–97. [[CrossRef](#)]
47. Roebuck, B.; Cox, D.; Reed, R. The temperature dependence of γ' volume fraction in a Ni-based single crystal superalloy from resistivity measurements. *Scr. Mater.* **2001**, *44*, 917–921. [[CrossRef](#)]
48. Caron, P. High γ' Solvus New Generation Nickel-Based Superalloys for Single Crystal Turbine Blade Applications. In Proceedings of the Superalloys 2000, Seven Springs Mountain Resort, Champion, PA, USA, 17–21 September 2000; Pollock, T.M., Kissinger, R.D., Bowman, R.R., Green, K.A., McLean, M., Olson, S., Schirra, J.J., Eds.; TMS: Warrendale, PA, USA, 2000; pp. 737–746. [[CrossRef](#)]
49. Mackay, R.; Gabb, T.P.; Garg, A.; Rogers, R.B.; Nathal, M. Influence of composition on microstructural parameters of single crystal nickel-base superalloys. *Mater. Charact.* **2012**, *70*, 83–100. [[CrossRef](#)]
50. Epishin, A.; Link, T.; Klingelhöffer, H.; Fedelich, B.; Brückner, U.; Portella, P. New technique for characterization of microstructural degradation under creep: Application to the nickel-base superalloy CMSX-4. *Mater. Sci. Eng. A* **2009**, *510–511*, 262–265. [[CrossRef](#)]
51. IMAGE J. Available online: <https://imagej.nih.gov/ij/> (accessed on 5 December 2020).
52. Hill, R. The Elastic Behaviour of a Crystalline Aggregate. *Proc. Phys. Soc. Sect. A* **1952**, *65*, 349–354. [[CrossRef](#)]
53. Morris, P.R. Elastic constants of polycrystals. *Int. J. Eng. Sci.* **1970**, *8*, 49–61. [[CrossRef](#)]
54. Matthies, S.; Humbert, M. On the Principle of a Geometric Mean of Even-Rank Symmetric Tensors for Textured Polycrystals. *J. Appl. Crystallogr.* **1995**, *28*, 254–266. [[CrossRef](#)]
55. Mura, T. *Micromechanics of Defects in Solids*; Springer: Dordrecht, The Netherlands, 1982.
56. Hill, R. Elastic properties of reinforced solids: Some theoretical principles. *J. Mech. Phys. Solids* **1963**, *11*, 357–372. [[CrossRef](#)]
57. Thomson, W. Elements of a mathematical theory of elasticity. *Philos. Trans. R. Soc. Lond.* **1856**, *146*, 481–498. [[CrossRef](#)]
58. Sutcliffe, S. Spectral Decomposition of the Elasticity Tensor. *J. Appl. Mech.* **1992**, *59*, 762–773. [[CrossRef](#)]
59. Mehrabadi, M.M.; Cowin, S.C. eigentensors of linear anisotropic elastic materials. *Q. J. Mech. Appl. Math.* **1990**, *43*, 15–41. [[CrossRef](#)]
60. Walpole, L.J. Fourth-rank tensors of the thirty-two crystal classes: Multiplication tables. *Proc. R. Soc. London. Ser. A Math. Phys. Sci.* **1984**, *391*, 149–179. [[CrossRef](#)]
61. Matthies, S.; Humbert, M. The Realization of the Concept of a Geometric Mean for Calculating Physical Constants of Polycrystalline Materials. *Phys. Status Solidi* **1993**, *177*, K47–K50. [[CrossRef](#)]
62. Brückner, U.; Epishin, A.; Nolze, G. Determination of the sign of the γ/γ' -misfit in nickel-base superalloys by use of spectral impure Cu(Cr) radiation. *Scr. Mater.* **1997**, *36*, 1279–1282. [[CrossRef](#)]